Distributed Antenna Tx/Rx Diversity Using Sparse Channel Estimation in Doubly Selective Nakagami-Rice Fading Channel

Jimmy Hadi SUSANTO† Hiroyuki MIYAZAKI† Katsuhiro TEMMA† and Fumiyuki ADACHI‡
Dept. of Communications Engineering, Graduate School of Engineering, Tohoku University
6-6-05 Aza-Aoba, Aramaki, Aoba-ku, Sendai, 980-8579 Japan
E-mail: †{jimmy, miyazaki, tenma}@mobile.ecei.tohoku.ac.jp, ‡adachi@ecei.tohoku.ac.jp

***Abstract*—Recently, we have studied frequency-domain space-time block coded joint transmit/receive diversity (FD-STBC-JTRD) for distributed antenna network (DAN). The channel of DAN can be modeled as doubly-selective (time- and frequency-selective) Nakagami-Rice fading channel. FD-STBC-JTRD requires accurate channel state information (CSI). However, in a high mobility environment, channel estimation is a problem. In this paper, we introduce sparse channel estimation scheme and evaluate, by computer simulation, the downlink throughput performance of DAN using FD-STBC-JTRD in a high mobility environment. It is shown that the sparse channel estimation works well even in a high mobility environment.**

Keywords—Distributed antenna network; Nakagami-Rice fading; transmit/receive diversity; channel estimation

I. INTRODUCTION

In next generation wireless communication systems, high data rate services are demanded even in high mobility environments. However, large transmit power is necessary to provide high data rate services. Distributed antenna network (DAN) [1]-[4] is one promising solution to solve this problem. A combination of DAN and frequency-domain space time block coded joint transmit/receive diversity (FD-STBC-JTRD) [5], [6] can significantly reduce transmit power [7]. In DAN, since some distributed antennas can be visible from a mobile terminal (MT), the channel becomes a doubly-selective (time- and frequency-selective) Nakagami-Rice fading. Recently, we have studied the potentiality of DAN using FD-STBC-JTRD in a high mobility environment [8]. FD-STBC-JTRD requires the accurate channel state information (CSI). However, in previous work, ideal channel estimation (CE) is assumed.

Cyclic delay pilot aided CE (CDP-CE) [9] using delay time domain windowing [10] can simultaneously estimate MIMO channels. However, in a doubly-selective Nakagami-Rice fading environment, there are noise only taps in the channel between the direct path and delay paths. In this paper, we introduce noise paths detection method [11] to CDP-CE (called sparse CDP-CE). We will show by computer simulation that sparse CDP-CE can improve CE accuracy due to noise paths removal and hence provides a good throughput performance in a high mobility environment.

The rest of the paper is organized as follows. System model is presented in Section II. This is followed by description of FD-STBC-JTRD time division duplex (TDD) transmission in Section III. Section IV describes sparse CDP-CE. In Section V, computer simulation results on the downlink throughput are discussed. Section VI offers some conclusions and future works.

II. SYSTEM MODEL

A. Linear DAN Model

In this paper, we consider high speed railway as a typical high mobility environment. Since MT can be assumed to move on one dimensional line, linear DAN model is used. Fig. 1 shows linear DAN model. Distributed antennas are linearly located at distance R intervals and connected to a signal processing center (SPC). Distributed antenna line and railway line are separated by βR. N_t distributed antennas closest to MT are selected as transmit antenna to form single frequency network (SFN). MT is assumed to be moving at a speed v and having N_r receive antennas.

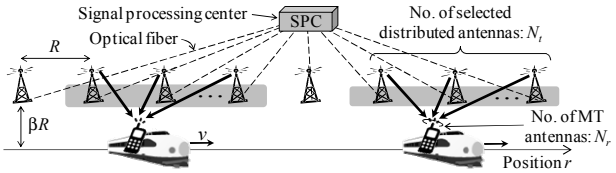

Fig. 1. Linear DAN model.

B. Doubly-Selective Nakagami-Rice Fading Model

In this paper, we consider doubly-selective Nakagami-Rice fading channel. Fig. 2 shows channel model in DAN between n-th distributed antenna and m-th MT antenna. The channel between each transmit-receive antenna pair is assumed to be composed of direct path and L delay paths. Each delay path consists of several unresolvable paths that scattered by circular scatterer clusters around each distributed antenna and arrives to MT from 360 degrees direction.

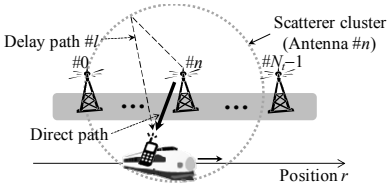

Fig. 2. Channel model.

978-1-4799-4449-1/14/$31.00 ©2014 IEEE

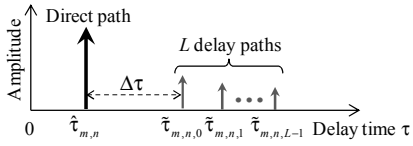

Fig. 3. Channel impulse response.

Fig. 3 shows channel impulse response between n-th distributed antenna and m-th MT antenna $h_{m,n}(\tau,t)$ expressed as

$$h_{m,n}(\tau,t)=\sqrt{\frac{K}{K+1}}\hat{h}_{m,n}(t)\delta\left(\tau-\hat{\tau}_{m,n}\right)+\sqrt{\frac{1}{K+1}}\sum_{l=0}^{L-1}\tilde{h}_{m,n,l}(t)\delta\left(\tau-\tilde{\tau}_{m,n,l}\right), \quad (1)$$

where K is defined as ratio between direct path power and delay paths average total power. $\hat{\tau}_{m,n}$ and $\tilde{\tau}_{m,n,l}$ denote delay time of direct path and l-th delay path between n-th distributed antenna and m-th MT antenna, respectively. $\hat{h}_{m,n}(t)$ and $\tilde{h}_{m,n,l}(t)$ are respectively complex-valued channel gains, including path loss, of direct path and l-th delay path between n-th distributed antenna and m-th MT antenna given as

$$\hat{h}_{m,n}(t)=\sqrt{u_n^{-a}}\hat{h}'_{m,n}(t), \quad (2)$$

$$\tilde{h}_{m,n,l}(t)=\sqrt{u_n^{-a}}\tilde{h}'_{m,n,l}(t), \quad (3)$$

where a is path loss exponent, and u_n is distance between n-th distributed antenna and MT. $\hat{h}'_{m,n}(t)$ and $\tilde{h}'_{m,n,l}(t)$ are respectively complex-valued channel gains of direct path and l-th delay path between n-th distributed antenna and m-th MT antenna that fluctuate due to fading.

The instantaneous received signal power $P_{r,n}(t)$ at MT from n-th distributed antenna can be expressed as

$$P_{r,n}(t)=p_{t,n}\cdot u_n^{-a}\cdot\frac{1}{K+1}\sum_{m=0}^{N_r-1}\left\{K\left|\hat{h}'_{m,n}(t)\right|^2+\sum_{l=0}^{L-1}\left|\tilde{h}'_{m,n,l}(t)\right|^2\right\}, \quad (4)$$

where $p_{t,n}$ is transmit power from n-th distributed antenna. Eq. (4) can be rewritten as

$$\begin{aligned}P_{r,n}(t)&=\left(p_{t,n}\cdot R^{-a}\right)\cdot\left(u_n/R\right)^{-a}\\&\quad\cdot\frac{1}{K+1}\sum_{m=0}^{N_r-1}\left\{K\left|\hat{h}'_{m,n}(t)\right|^2+\sum_{l=0}^{L-1}\left|\tilde{h}'_{m,n,l}(t)\right|^2\right\}\\&=P_{t,n}\cdot U_n^{-a}\cdot\frac{1}{K+1}\sum_{m=0}^{N_r-1}\left\{K\left|\hat{h}'_{m,n}(t)\right|^2+\sum_{l=0}^{L-1}\left|\tilde{h}'_{m,n,l}(t)\right|^2\right\}\end{aligned}, \quad (5)$$

where $P_{t,n}=p_{t,n}\cdot R^{-a}$ is the normalized transmit power and $U_n=u_n/R$ is the normalized distance between n-th distributed antenna and MT.

III. FD-STBC-JTRD TDD Transmission

In this paper, we consider TDD transmission using FD-STBC-JTRD. Fig. 4 shows the frame structure. To simplify MT structure and reduce CSI feedback, CE and FDE are performed at SPC. First, uplink data contains N_b blocks and 2 pilot blocks that are inserted in both ends of uplink data block

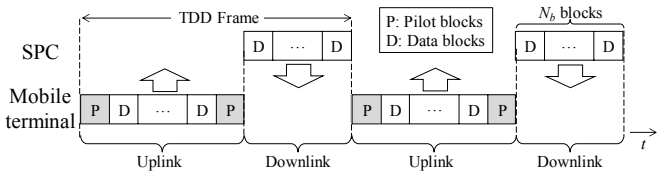

Fig. 4. TDD frame structure.

are transmitted from MT. Then, CE is performed in each pilot stage by using N_p previous pilot blocks at SPC. After that, uplink and downlink channel are predicted by using inter/extrapolation [12]. Finally, uplink data detection and FD-STBC-JTRD downlink transmission are performed by using predicted uplink and downlink channel, respectively.

A. FD-STBC-JTRD Encoding

Fig. 5 illustrates transmitter/receiver structure of FD-STBC-JTRD. Throughout the paper, the T_s symbol-spaced discrete time representation is used. In FD-STBC-JTRD, signal processing is performed in each symbol block. In this paper, we use channel gains of the center point of each block to perform FD-STBC-JTRD. The channel gain of direct path and l-th delay path between n-th distributed antenna and m-th MT antenna are denoted by $\hat{h}_{m,n}$ and $\tilde{h}_{m,n,l}$, respectively. At SPC, a sequence of $J\times N_c$ data modulated symbols is divided into a sequence of J blocks of N_c symbols each. N_c-point fast Fourier transform (FFT) is applied to convert the j-th symbol block $\{d_j(t);\ t=0,...,N_c-1,\ j=0,...,J-1\}$ into frequency-domain signal $\{D_j(k);\ k=0,...,N_c-1, j=0,...,J-1\}$.

STBC encoding is applied to obtain $N_t\times Q$ frequency-domain signal block $\mathbf{\Omega}(k)$. STBC encoding matrix $\mathbf{\Omega}(k)$ is given as

$$\mathbf{\Omega}(k)=\left(D_0(k)\right), \quad \text{for } N_t=1, \quad (6)$$

$$\mathbf{\Omega}(k)=\begin{pmatrix}D_0(k) & -D_1^*(k)\\ D_1(k) & D_0^*(k)\end{pmatrix}, \quad \text{for } N_t=2, \quad (7)$$

$$\mathbf{\Omega}(k)=\begin{pmatrix}D_0(k) & -D_1^*(k) & -D_2^*(k) & 0\\ D_1(k) & D_0^*(k) & 0 & -D_2^*(k)\\ D_2(k) & 0 & D_0^*(k) & D_1^*(k)\end{pmatrix}. \text{for } N_t=3. \quad (8)$$

After STBC encoding, transmit FDE is applied. N_t streams of Q coded frequency-domain signal block $\mathbf{X}(k)$ of size $N_t\times Q$ after transmit FDE can be expressed using matrix form as

$$\mathbf{X}(k)=C\mathbf{W}^H(k)\mathbf{\Omega}(k), \quad (9)$$

where C is the power normalization factor, to keep the average transmit power constant, given as

$$C=\sqrt{N_c\Big/\sum_{n=0}^{N_t-1}\sum_{m=0}^{N_r-1}\sum_{k=0}^{N_c-1}\left|W_{m,n}(k)\right|^2}, \quad (10)$$

where $W_{m,n}(k)$ is the element of transmit FDE matrix $\mathbf{W}(k)$. In this paper, we use the following weight [13]

$$W_{m,n}(k)=H_{m,n}(k)\Big/\left(\frac{1}{N_r}\sum_{n=0}^{N_t-1}\sum_{m=0}^{N_r-1}\left|H_{m,n}(k)\right|^2+\frac{2N_0}{T_s}\right), \quad (11)$$

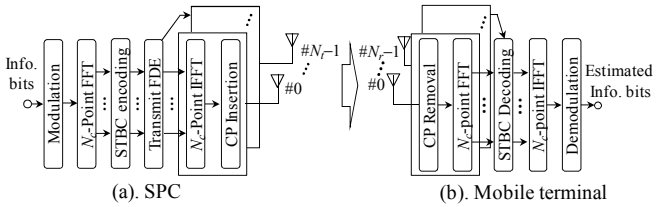

Fig. 5. FD-STBC-JTRD transmission model.

where $2N_0/T_s$ is variance of additive white Gaussian noise (AWGN) and N_0 is the one-sided power spectrum density of AWGN. $H_{m,n}(k)$ denotes frequency-domain transfer function of the channel between n-th distributed antenna and m-th MT antenna given as

$$H_{m,n}(k)=\sqrt{\frac{2E_s}{T_s}}\left\{\begin{array}{l}\sqrt{\frac{K}{K+1}}\hat{h}_{m,n}\exp\left(-j2\pi k\hat{\tau}_{m,n}/N_c\right)+\\ \sqrt{\frac{1}{K+1}}\sum_{l=0}^{L-1}\tilde{h}_{m,n,l}\exp\left(-j2\pi k\tilde{\tau}_{m,n,l}/N_c\right)\end{array}\right\}, \quad (12)$$

where E_s denotes transmit symbol energy. Finally, N_c-point inverse FFT (IFFT) is applied to obtain time-domain codeword. After inserting the cyclic prefix (CP) of N_g symbols into the guard interval (GI), N_t streams of (N_c+N_g) symbol blocks each are transmitted from N_t distributed antennas.

B. FD-STBC-JTRD Decoding

At MT, after CP removal, N_r received signals are transformed into frequency-domain signals by N_c-point FFT. Frequency-domain received signal in q-th time-slot and m-th antenna can be expressed as

$$Y_{m,q}(k)=\sum_{n=0}^{N_t-1}H_{m,n}(k)X_{n,q}(k)+\Pi_{m,q}(k), \quad (13)$$

where $X_{n,q}(k)$ is frequency-domain transmitted signal from n-th distributed antenna at q-th time-slot, and $\Pi_{m,q}(k)$ is AWGN with zero mean and variance $2N_0/T_s$. Then, in each frequency component, STBC decoding is carried out. STBC decoded j-th received symbol block $\{\hat{D}_j(k)\ ;\ k=0,...,N_c-1,\ j=0,...,J-1\}$ is given as

$$\left(\hat{D}_0(k)\right)=\left(Y_{0,0}(k)\right), \quad \text{for } N_r=1, \quad (14)$$

$$\left(\begin{array}{c}\hat{D}_0(k)\\ \hat{D}_1(k)\end{array}\right)=\left(\begin{array}{c}Y_{0,0}(k)+Y_{1,1}^*(k)\\ Y_{1,0}(k)-Y_{0,1}^*(k)\end{array}\right), \quad \text{for } N_r=2, \quad (15)$$

$$\left(\begin{array}{c}\hat{D}_0(k)\\ \hat{D}_1(k)\\ \hat{D}_2(k)\end{array}\right)=\left(\begin{array}{c}Y_{0,0}(k)+Y_{1,1}^*(k)+Y_{2,2}^*(k)\\ Y_{1,0}(k)-Y_{0,1}^*(k)+Y_{2,3}^*(k)\\ Y_{2,0}(k)-Y_{0,2}^*(k)-Y_{1,3}^*(k)\end{array}\right). \quad \text{for } N_r=3. \quad (16)$$

Finally, N_c-point IFFT is applied and data detection is performed to each symbol block.

IV. Sparse CDP-CE

In FD-STBC-JTRD, high accurate MIMO CE is required to perform transmit FDE. CDP-CE can simultaneously estimate MIMO channel while suppressing pilot insertion loss. However, CDP-CE uses fixed delay time-domain window. Therefore, in sparse channel, e.g. doubly-selective Nakagami-Rice fading, CE accuracy degrades due to noise paths which remain in zero-valued taps. Fig. 6 illustrates channel impulse response of sparse doubly-selective Nakagami-Rice fading channel. To improve CE accuracy, we introduce sparse CDP-CE. In sparse CDP-CE, noise paths are detected by using channel time correlation property [11]. Since the time correlation of active paths (direct path and delay paths) is usually higher than that of noise paths, noise paths can be detected accurately by setting correlation threshold properly. Here, without any loss of generality, we focus on CE which is performed in previous $i(i=0,..,N_p-1)$-th pilot block.

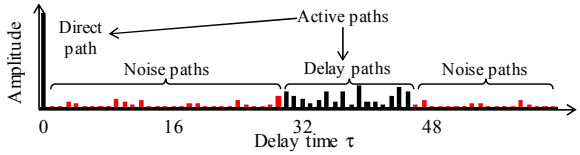

Fig. 6. Nakagami-Rice fading impulse response.

At MT, cyclic delay is applied to pilot blocks to be transmitted from all MT antennas. The i-th pilot block transmitted from m-th MT antenna before CP insertion $\psi_m^{(i)}(t)$ can be expressed as

$$\psi_m^{(i)}(t)=\psi^{(i)}((t-\Delta m)\bmod N_c), \quad (17)$$

where Δ is the unit cyclic delay $(N_g\le\Delta\le N_c/N_t)$, which is an integer of multiple GI length. Frequency-domain representation of i-th cyclic delayed pilot block transmitted from m-th MT antenna is given as

$$\begin{aligned}\Psi_m^{(i)}(k)&=\frac{1}{\sqrt{N_c}}\sum_{t=0}^{N_c-1}\psi_m^{(i)}(t)\exp\left(-j2\pi kt/N_c\right)\\ &=\Psi^{(i)}(k)\exp\left(-j2\pi k\Delta m/N_c\right)\end{aligned}, \quad (18)$$

where $\Psi^{(i)}(k)$ is the k-th frequency component of $\psi^{(i)}(t)$, and $\exp(\cdot)$ is the phase rotation term as a result of cyclic delay. After inserting CP of N_g symbols into GI, cyclic delayed pilot blocks are transmitted from all MT antennas.

Fig. 7 shows channel estimator structure of sparse CDP-CE. At SPC, i-th received pilot block at n-th distributed antenna after CP removal $\xi_n^{(i)}(t)$ can be expressed as

$$\xi_n^{(i)}(t)=\sqrt{\frac{2E_s}{T_s}}\sum_{m=0}^{N_t-1}\left\{\begin{array}{l}\sqrt{\frac{K}{K+1}}\hat{h}_{m,n}^{(i)}\psi_m^{(i)}(t-\hat{\tau}_{m,n}^{(i)})+\\ \sqrt{\frac{1}{K+1}}\sum_{l=0}^{L-1}\tilde{h}_{m,n,l}^{(i)}\psi_m^{(i)}(t-\tilde{\tau}_{m,n,l}^{(i)})\end{array}\right\}+\eta_n^{(i)}(t), \quad (19)$$

where $\eta_n^{(i)}(t)$ represents AWGN at n-th distributed antenna when i-th pilot block is received. Then N_c-point FFT is applied

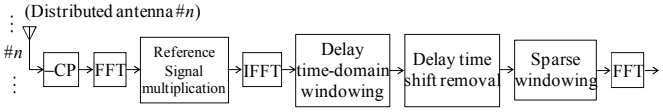

Fig. 7. Sparse CDP-CE channel estimator.

to convert the received pilot blocks into frequency-domain. The k-th frequency component of i-th received pilot block at n-th distributed antenna $\Xi_n^{(i)}(k)$ can be expressed as

$$\begin{aligned}\Xi_n^{(i)}(k) &= \frac{1}{\sqrt{N_c}}\sum_{t=0}^{N_c-1}\xi_n^{(i)}(t)\exp\left(-j2\pi kt/N_c\right)\\ &= \sum_{m=0}^{N_r-1}H_{m,n}^{(i)}(k)\Psi_m^{(i)}(k)+\Pi_n^{(i)}(k)\\ &= \left\{\sum_{m=0}^{N_r-1}H_{m,n}^{(i)}(k)\exp\left(-j2\pi k\Delta m/N_c\right)\right\}\Psi^{(i)}(k)+\Pi_n^{(i)}(k)\end{aligned}, \tag{20}$$

where $H_{m,n}^{(i)}(k)$ and $\Pi_n^{(i)}(k)$ denote k-th frequency component of channel transfer function between m-th MT antenna and n-th distributed antenna at i-th pilot block, including transmit power, and AWGN at n-th distributed antenna, respectively. Here, composite channel transfer function $H_n^{(i)}(k)$ is defined as

$$H_n^{(i)}(k)=\sum_{m=0}^{N_r-1}H_{m,n}^{(i)}(k)\exp\left(-j2\pi k\Delta m/N_c\right). \tag{21}$$

Then, frequency-domain received pilot blocks are multiplied with reference signal to estimate composite channel transfer function. In this paper, zero-forcing (ZF) weight is used as reference signal. Composite channel transfer function can be estimated as

$$\bar{H}_n^{(i)}(k)=\sum_{m=0}^{N_r-1}H_{m,n}^{(i)}(k)\exp\left(-j2\pi k\Delta m/N_c\right)+\frac{\left\{\Psi^{(i)}(k)\right\}^*}{\left|\Psi^{(i)}(k)\right|^2}\Pi_n^{(i)}(k) \tag{22}$$

.

Applying N_c-point IFFT to $\bar{H}_n^{(i)}(k)$, we can obtain composite channel impulse response $\bar{h}_n^{(i)}(\tau)$ given as

$$\begin{aligned}\bar{h}_n^{(i)}(\tau) &= \sqrt{\frac{2E_s}{T_s}}N_c\sum_{m=0}^{N_r-1}\left\{\begin{array}{l}\sqrt{\frac{K}{K+1}}\hat{h}_{m,n}^{(i)}\delta\left(\tau-\hat{\tau}_{m,n}^{(i)}-\Delta m\right)+\\ \sqrt{\frac{1}{K+1}}\sum_{l=0}^{L-1}\tilde{h}_{m,n,l}^{(i)}\delta\left(\tau-\tilde{\tau}_{m,n,l}^{(i)}-\Delta m\right)\end{array}\right\}\\ &+\frac{1}{\sqrt{N_c}}\sum_{k=0}^{N_c-1}\frac{\left\{\Psi^{(i)}(k)\right\}^*}{\left|\Psi^{(i)}(k)\right|^2}\Pi_n^{(i)}(k)\exp\left(j2\pi k\tau/N_c\right)\end{aligned}. \tag{23}$$

As shown in Eq. (23), estimated composite channel impulse response is in delay time-domain. Therefore, by applying delay time-domain windowing channel impulse response can be obtained as

$$\bar{h}_{m,n}^{(i)}(\tau)=\begin{cases}\bar{h}_n^{(i)}(\tau+\Delta m) & \text{if } 0\le\tau\le\Delta\\ 0 & \text{otherwise}\end{cases}. \tag{24}$$

By applying delay time-domain window, channel impulse response from each MT antenna can be separated. However, noise only taps still remain, and hence, it leads to CE accuracy degradation. To remove noise paths, we introduce noise paths detection method by using channel time correlation, which can be calculated from N_p previous pilot blocks. The τ-th channel tap time correlation of impulse response between n-th distributed antenna and m-th MT antenna at i-th pilot block is given as

$$\rho_{m,n}^{(i)}(\tau)=\frac{1}{N_p}\sum_{i'=0}^{N_p-1}\bar{h}_{m,n}^{(i-i')}(\tau)\bar{h}_{m,n}^{(i-i'-1)*}(\tau). \tag{25}$$

Then, the threshold value is calculated by averaging absolute value of time correlation as

$$\rho_{th}^{(i)}=\frac{\varepsilon}{\Delta}\sum_{\tau=0}^{\Delta-1}\left|\rho_{m,n}^{(i)}(\tau)\right|, \tag{26}$$

where ε is threshold coefficient, which is used to adjust threshold value. Finally, noise paths can be detected by comparing absolute value of time correlation of each tap $\left|\rho_{m,n}^{(i)}(\tau)\right|$ with threshold value $\rho_{th}^{(i)}(\tau)$ as

$$\bar{\bar{h}}_{m,n}^{(i)}(\tau)=\begin{cases}\bar{h}_{m,n}^{(i)}(\tau) & \text{if } \left|\rho_{m,n}^{(i)}(\tau)\right|\ge\rho_{th}^{(i)}\\ 0 & \text{otherwise}\end{cases}. \tag{27}$$

By introducing noise paths detection method to CDP-CE, delay time-domain window width can be adaptively controlled in sparse channel, and therefore CE accuracy can be improved.

V. Simulation Results

In this section, downlink throughput performance of DAN using FD-STBC-JTRD in a high mobility environment is evaluated by computer simulation. We consider QPSK data modulation, an FFT block size of N_c=512 symbols, and a GI of N_g=64 symbols. The channel is assumed to be doubly-selective Nakagami-Rice fading which is composed of direct path and L=16 delay paths having uniform power delay profile, delay time gap between direct path and first delay path is $\Delta\tau$=30 symbols, and path loss exponent is a=3.5. We assume that K-factor of all channel between each transmit-receive antenna pair is K=5 [14]. No. of transmit and receive antennas N_t=N_r=2 are assumed. For sparse CDP-CE, we use Chu sequence [15] as pilot signal, which is inserted in every N_b data blocks.

A. Impact of Threshold Coefficient

Fig. 8 shows impact of threshold coefficient ε on throughput performance of DAN using FD-STBC-JTRD when sparse CDP-CE is employed. As can be seen, when ε=0 all channel taps are detected as active paths, and hence sparse CDP-CE performs as conventional CDP-CE. As ε increases, throughput performance is improved as a result of noise paths removal. From Fig. 8 it can be seen that sparse CDP-CE performs optimally when ε=0.1~0.2. Moreover, when ε further increases some active paths are treated as noise paths due to high threshold value, therefore throughput performance degrades. To achieve optimum performance ε =0.1 is used in next simulation.

B. Application of Sparse CDP-CE in DAN

Fig. 9 shows downlink throughput performance of DAN using FD-STBC-JTRD when sparse CDP-CE is used. For comparison, throughput performance in ideal CE scheme, noise paths are perfectly removed scheme (noted as ideal sparse

CDP-CE), and conventional CDP-CE scheme are also shown. As can be seen from Fig. 9, the required transmit power to achieve target throughput can be reduced by applying sparse CDP-CE compared to conventional CDP-CE due to noise paths removal. For example when the target throughput is 1bps/Hz, sparse CDP-CE can reduce transmit E_s/N_0 by about 2dB. Fig. 10 shows impact of maximum Doppler frequency on sparse CDP-CE. Assuming 10MHz signal bandwidth at the carrier frequency 2GHz, the normalized maximum Doppler frequency $f_D T_s=10^{-4}$ corresponds to a speed of 540km/h. It is seen from Fig. 10 that sparse CDP-CE can improve CE accuracy by about 1.3 times compared to conventional CDP-CE even in a high mobility environment.

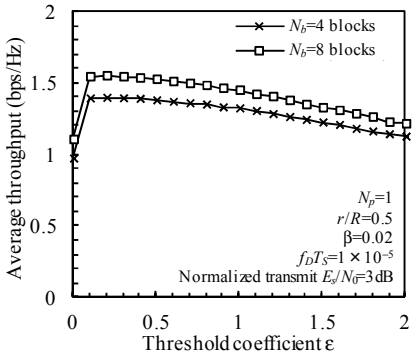

Fig. 8. Impact of threshold coefficient.

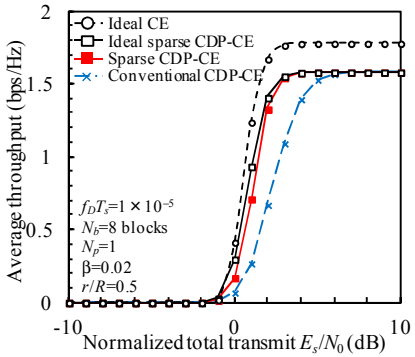

Fig. 9. Sparse CDP-CE application to DAN.

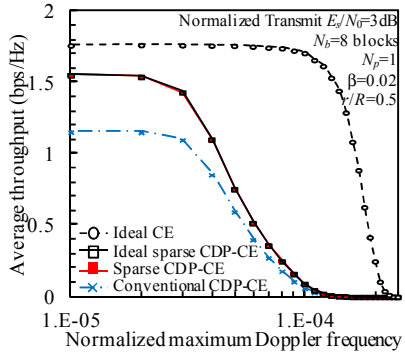

Fig. 10. Impact of maximum Doppler frequency.

VI. CONCLUSIONS

In this paper, we introduced sparse CDP-CE to DAN using FD-STBC-JTRD. It was shown that sparse CDP-CE can improve CE accuracy due to noise paths removal, and hence provides a good throughput performance even in a high mobility environment. In this paper, non-adaptive threshold coefficient is used. Technique to control threshold coefficient adaptively is practically important future work. Investigating the impact of TDD frame length and improving tracking ability of sparse CDP-CE against time-selective fading are also left as our future works.

REFERENCES

[1] A. A. M. Saleh, A. J. Rustako, and R. S. Roman, "Distributed antennas for indoor radio communications," IEEE Trans. Commun. vol.35, no.12, pp.1245-1251, Dec. 1987.

[2] W. Choi and J. G. Andrews, "Downlink performance and capacity of distributed antenna systems in a multicell environment," IEEE Trans. Wireless Commun., vol.6, no.1, pp.69-73, Jan. 2007.

[3] E. Kudoh and F. Adachi, "Study of a multi-hop communication in a virtual cellular system," Proc. 6th International Symposium on Wireless Personal Multimedia Communications, vol.3, pp.261-265, Yokosuka, Japan, Oct. 2003.

[4] H. Matsuda, H. Tomeba, and F. Adachi, "Channel capacity of distributed antenna system using maximal ratio transmission," Proc. 5th IEEE VTS APWCS, Sendai, Japan, Aug. 2008.

[5] H. Tomeba, K. Takeda, and F. Adachi, "Space-time block coded-joint transmit/receive diversity in a frequency-nonselective Rayleigh fading channel," IEICE Trans. Commun., vol.E89, no.8, pp.2189-2195, Aug. 2006.

[6] H. Tomeba, K. Takeda, and F. Adachi, "Space-time block coded-joint transmit/receive diversity using more than 4 receive antennas," Proc. 68th IEEE VTC, Calgary, Canada, Sep. 2008.

[7] R. Matsukawa, T. Obara, K. Takeda, and F. Adachi, "Downlink throughput performance of distributed antenna network using transmit/receive diversity," Proc. 74th IEEE VTC, San Francisco, US, Sep. 2011.

[8] J. H. Susanto, H. Miyazaki, K. Temma, T. Yamamoto, T. Obara, and F. Adachi, "Linearly distributed antenna diversity using single frequency network for high-speed railway communications," Proc. 19th IEEE APCC, Bali, Indonesia, Aug. 2013.

[9] T. Fujimori, K. Takeda, K. Ozaki, A. Nakajima, and F. Adachi, "Channel estimation using cyclic delay pilot for SC-MIMO multiplexing," IEICE Trans. Commun., vol.E91-B, no.9, pp.2925-2932, Sep. 2008.

[10] J. J. de Beek, O. Edfors, M. Sandell, S. K. Wilson, and P. O. Borjesson, "On channel estimation in OFDM systems," Proc. 1995 VTC, vol.2, pp.815-819, Jul. 1995.

[11] F. Wan, W. P. Zhu, and M. N. S. Swamy, "Semi-blind most significant tap detection for sparse channel estimation of OFDM systems," IEEE Trans. on Circuits and Systems I, Reg. Paper, vol.57, no.3, pp.703-713, Mar. 2010.

[12] S. Yoshioka, S. Kumagai, T. Yamamoto, T. Obara, and F. Adachi, "Single-carrier STBC diversity using CDP-CE and linear inter/extra-polation in a doubly selective fading channel," Proc. 10th IEEE VTS APWCS, Seoul, Korea, Aug. 2013.

[13] H. Tomeba, K. Takeda, and F. Adachi, "Frequency-domain space time block coded-joint transmit/receive diversity for the single carrier transmission," Proc. 10th IEEE ICCS, Singapore, Oct. 2006.

[14] J. Lu, G. Zhu, and B. Ai, "Fading analysis for the high speed railway viaduct and terrain cutting scenarios," International Journal of Antennas and Propagation, vol.2012, doi:10.1155/2012/862945, 2012.

[15] D. C. Chu, "Polyphase codes with good periodic correlation properties," IEEE Trans. Inf. Theory, vol.18, no.4, pp.531-532, Jul. 1972.